

Inhibitory Mechanism of Prenylated Flavonoids Isolated from Mulberry Leaves on α -Glucosidase by Multi-Spectroscopy and Molecular Dynamics Simulation

Jin-Long Tian,^{||} Min Zhao,^{||} Jing-Yi Xu, Tian-Meng Lv, Xiao-Chang Liu, Sheng Sun, Qi Guan, Zhen-Chi Zhou, Jie Wu, Ming-Yue Zhao, Yue Li, Han-Xiao Liu, Sheng-Li Niu,* and Ping Hu*



Cite This: *J. Agric. Food Chem.* 2023, 71, 9135–9147



Read Online

ACCESS |



Metrics & More



Article Recommendations



Supporting Information

ABSTRACT: Flavonoids have always been considered as the chemical basis for the hypoglycemic effect of mulberry leaves. In the course of our search for hypoglycemic effect agents from natural sources, a systematic study was launched to explore prenylated flavonoids from mulberry leaves. Herein, chemical investigation led to the isolation of 10 characteristic prenylated flavonoids, including two new compounds (1 and 3). Their structures were elucidated based on spectroscopic data. All compounds exhibited good α -glucosidase inhibitory activity *in vitro*, among which compound 2 had the best activity ($IC_{50} = 2.6 \mu M$), better than acarbose ($IC_{50} = 19.6 \mu M$). Additional *in vivo* tests have further demonstrated compound 2 has a good ability to reduce postprandial blood glucose. Then, multi-spectroscopic methods and molecular simulation studies were used to study the inhibition mechanism. The results showed that compound 2 was a mixed inhibition of α -glucosidase and the binding process was spontaneous, with van der Waals forces as the main driving force, followed by hydrogen bonding and electrostatic forces. The above studies enriched the chemical basis of mulberry leaves, and the application of computational chemistry also provided a reference for future research on such structures.

KEYWORDS: *Morus alba*, mulberry leaves, prenylated flavonoid, α -glucosidase, molecular dynamics

1. INTRODUCTION

Diabetes mellitus (DM) is a common endocrine metabolic disorder accompanied by glucose, fat, and protein metabolism disorders caused by insulin secretion and/or functional deficiencies.¹ The global prevalence of DM is growing rapidly, and the number of patients with diabetes is estimated to be 463 million in 2019, which is expected to increase to 578 million by 2030 and 700 million by 2045.² Without effective treatment, diabetes mellitus (DM) will result in severe complications in various body tissues or organs, such as liver dysfunction, renal failure, blindness, and nervous system damage.³ This situation will cause a huge health and economic burden to individuals and society. Consequently, the prevention and treatment of DM is urgent. Hypoglycemic drugs with various mechanisms and targets have been discovered to lower the level of blood glucose as the pathological mechanism, and effective therapeutic approaches for the disease have become more and more clear.⁴ Acarbose is a commonly used α -glucosidase inhibitor, which is mainly used to reduce postprandial hyperglycemia. α -Glucosidase is a carbohydrate hydrolase that plays a key role in the absorption of carbohydrates in the small intestine. It has been recognized as a therapeutic target for regulating postprandial hyperglycemia.⁵ Although hypoglycemic drugs play an important role in blood glucose management, they usually have side effects or limitations. People gradually realize that in addition to drugs to reduce blood glucose levels, daily dietary control is also crucial. Dietary and plant-derived products have been tested in many preclinical and clinical trials

for their anti-diabetic activities in recent years.⁶ Some natural functional ingredients in food can not only reduce hyperglycemia but also have fewer side effects than currently used drugs and can provide nutritional benefits for diabetics.⁷

Morus alba L., a deciduous tree known as white mulberry belonging to the family of Moraceae, is widely distributed in South Europe, Southeast Asia, and Middle North America.⁸ There are about 19 species in the genus *Morus*, of which white mulberry is the most commonly grown and widely studied one.^{9,10} In China, there are approximately 15 species of genus *Morus*, so it has the largest number of mulberry species in the world.¹¹ *M. alba* (white mulberry) is a kind of valuable traditional medicine and also functional food. The different parts of *M. alba* have been commonly used in the traditional Chinese medicine for various therapeutic effects¹⁰ and its leaves, branches, fruits, and root bark were all included in 2020 edition of the Chinese Pharmacopoeia.¹² The dry leaves of *M. alba* (white mulberry leaves, mulberry leaves, Mori Folium) could clear the lungs and moisten their dryness, clear the liver, and brighten the eyes. Hence, they are used to treat inflammation, hypertension, and diabetes.¹⁰ Mulberry leaves are also a type of food raw

Received: February 8, 2023

Revised: May 5, 2023

Accepted: May 15, 2023

Published: June 2, 2023



material, and numerous studies have been conducted on their development and application in food, including ordinary food, health food, drinks, and condiments.¹¹ In recent years, research works have found that foods containing mulberry leaves can regulate hyperglycemia. Mulberry leaf tea offers antioxidant properties as well as the ability to reduce blood glucose levels. In Japan and Korea, patients with diabetes take mulberry leaf supplements in order to regulate their blood glucose.¹³ With more investigation, it has been shown that flavonoids are the key bioactive components of mulberry leaves that can help with diabetes. The hypoglycemic mechanisms of flavonoids from mulberry leaves include inhibiting α -glucosidase and α -amylase to prolong carbohydrate digestion, inhibiting PTP1B over-expression, activating the AMPK pathway, and so on.¹⁴

These investigations showed that flavonoids in mulberry leaves controlled blood glucose through a number of ways. Simple substituent flavonoids from mulberry leaves (methoxylation, hydroxylation, glycosidation, etc.) have traditionally been thought to constitute the chemical foundation for the hypoglycemic action, but there are few studies on the structure of prenylated flavonoids in mulberry leaves. Based on this, in this present research, we explored the prenylated flavonoid constituents of mulberry leaves, the relationship between prenylated flavonoids and α -glucosidase inhibitory activity, and possible inhibitory modes by multispectroscopic and molecular dynamics methods.

2. MATERIALS AND METHODS

2.1. Materials and Instruments. Optical rotations were measured on a polarimeter (DIP-370) by Jasco (MD, USA). ECD spectra were acquired using a Bio-Logic MOS 450 spectrometer (Claix, France). The HR-ESI-MS spectra were recorded on an Agilent 6550 Q-TOF mass spectrometer (Agilent Technologies, Inc., Santa Clara, California, USA). The NMR spectra were recorded on a Bruker ARX-400 spectrometer (Bruker Corporation, Bremen, Germany). The UV spectra were acquired using a UV-1700 spectrophotometer (Shimadzu, Tokyo, Japan). The FT-IR spectra were acquired using a Bruker Tensor-27 spectrometer (Bruker Corporation, Karlsruhe, Germany). Sephadex LH-20 (GE Healthcare, Uppsala, Sweden), silica gel (200–300 mesh, Qingdao Marine Chemical Co., Ltd., Qingdao, China), and RP-C₁₈ (50 μ m, YMC Co., Ltd., Kyoto, Japan) were used for column chromatography (CC). The compounds were acquired by an Agilent 1260 HPLC with a DAD detector (Agilent Technologies, Inc., Santa Clara, California, USA). Acarbose were obtained from Nanjing Plant Origin Biological Technology Co., Ltd. (Nanjing, Jiangsu, China), and *p*-nitrophenyl- α -glucopyranoside (*p*-NPG) and α -glucosidase were obtained from Sigma-Aldrich (St Louis, MO, USA).

2.2. Plant Material. The leaves of *Morus alba* (Moraceae) were supplied by Anguo Market (Anguo City, Hebei Province, China) in October 2018. The authentication of the plant sample was achieved by Prof. Wei Ning, who is from the School of Horticulture, Shenyang Agricultural University. The voucher specimen (no. MA-20181001) was deposited in the College of Animal Science and Veterinary Medicine, Shenyang Agricultural University.

2.3. Extraction and Isolation. Air-dried mulberry leaves (25.5 kg) were refluxed three times with 95% EtOH, and the solvent was evaporated under reduced pressure to obtain a crude residue. The residue was suspended in distilled water (H₂O, 7 L) and successively extracted from the aqueous solution by use of petroleum ether (PE, 3 \times 7 L), ethyl acetate (EtOAc, 3 \times 7 L), and *n*-butanol (BuOH, 3 \times 7 L). A EtOAc-soluble fraction from mulberry leaves exhibited strong α -glucosidase inhibitory activity (IC₅₀ = 19.4 \pm 2.8 mg/L). The EtOAc layer was further concentrated to dryness, and the lipophilic crude extract (650 g) was passed over silica gel CC, eluting with a gradient mixture solvent system of *n*-hexane–acetone in increasing polarity (100:0, 100:5, 100:10, 100:15, and 100:20) (Scheme S1). A total of 15 main fractions (A–O) were obtained on the basis of the TLC profiles,

which were monitored by ultraviolet light at 254 nm. The main fraction B was roughly separated by silica gel CC using 3, 5, and 10% EtOAc in *n*-hexane as the mobile phase to afford 11 sub-fractions (B1–B11). Fraction B6 was roughly isolated by Sephadex LH-20 column and eluted with a 50% CHCl₃ in MeOH to obtain seven fractions (B6a–B6g). Fraction B6d was further purified through an ODS reverse-phase column eluted with 60, 70, and 80% methanol in water to yield 1 (4.5 mg). Fraction B6f was subjected to preparative TLC (PTLC) using 10% EtOAc in PE as the developing solvent to provide 3 (4.9 mg). The main fraction D was first fractionated via a silica gel column using a gradient mixture of *n*-hexane–acetone (10:1, 7:1, and 5:1 v/v) to obtain 10 subfractions (D1–D10). The subfraction D6 was subjected to an ODS reverse-phase column eluted with 60, 70, and 85% methanol in water to give seven fractions (D6a–D6g) based on TLC analysis. The third subfraction D6c was further purified by semi-preparative HPLC using acetonitrile (ACN)-H₂O with a 0.1% trifluoroacetic acid (TFA) gradient (50:50–90:10, v/v) as the mobile phase to afford 8 (6.9 mg, *t*_R = 29.3 min, 3 mL/min). Subfraction D6e was repeatedly recrystallized using 10% acetone in PE as the mixture solvent to yield 10 (6.4 mg). The major fraction F was separated through a Sephadex LH-20 column eluted with 50% MeOH in CH₂Cl₂ to obtain 11 major fractions (F1–F11) based on the TLC profiles. Subfraction F7 was separated by semi-preparative HPLC using ACN-H₂O with 0.1% TFA gradient (30:70–80:20, v/v) as the eluent to gain 4 (6.7 mg, *t*_R = 31.5 min, 3 mL/min) and 5 (7.3 mg, *t*_R = 40.2 min, 3 mL/min), respectively. Subfraction F7 was further subjected to PTLC using 10% EtOAc in PE developing solvent, yielding compound 2 (5.3 mg). The major fraction H was rechromatographed on a silica gel column, eluting with 10% acetone in *n*-hexane to generate 10 subfractions (H1–H10). Subfraction H5 was further separated by semi-preparative HPLC by use of ACN-H₂O with 0.1% TFA gradient (30:70–90:10, v/v) as the mobile phase to obtain 6 (6.2 mg, *t*_R = 33.2 min, 3 mL/min) and 7 (5.5 mg, *t*_R = 38.3 min, 3 mL/min), respectively. Subfraction H6 was subsequently isolated using a Sephadex LH-20 column eluted with MeOH, and the main fraction was further repeatedly recrystallized using 10% EtOAc in PE to give 9 (3.8 mg).

2.4. α -Glucosidase Inhibitory Activity Assay. Assays were performed by existing methods using 96-well microtiter plates. First, we used DMSO to dissolve and dilute the compounds to corresponding concentrations. Acarbose was selected as the positive control and has been used in our previous work.¹⁵ Then, α -glucosidase (10 U/mg) derived from *Saccharomyces cerevisiae* was dissolved in 0.5 U/mL PBS solution at pH 6.8 and *p*-nitrophenyl α -D-glucopyranoside (*p*-NPG) substrate dissolved to 5 mM. Each assay well includes the sample (10 μ L), an enzyme (20 μ L), and PBS (110 μ L). Each blank well includes PBS (130 μ L) and the sample (10 μ L). After careful shaking to mix thoroughly, the 96-well plate was stored at 37 °C for 15 min. Next, *p*-NPG (20 μ L) was added to each well, and then the solution was incubated at 37 °C for an additional 15 min. The reaction was then stopped by adding 0.2 M sodium carbonate (100 μ L). To quantify the hydrolysate, the 405 nm OD value was evaluated and assayed in triplicate for each concentration of the sample. The final step is to calculate the IC₅₀ values and related representations as mean \pm standard deviation.

2.5. Inhibition Kinetics. Kinetic studies of flavonoids on α -glucosidase were performed using the Lineweaver–Burk equation. Twenty microliters of α -glucosidase (0.5 U), 130 μ L of PBS solution, and 10 μ L of flavonoids (0–0.625 μ M) were mixed and incubated at 37 °C for 5 min. Afterward, 40 μ L of *p*-NPG (0.25–6 mM) was added and incubated in 96-well plates at 37 °C. The absorbance was measured every minute at 405 nm using an enzyme marker.

2.6. Fluorescence Quenching Analysis. The fluorescence spectra at 300–500 nm were measured using an RF6000 fluorescence spectrometer (Shimadzu, Japan). The α -glucosidase (0.1 U) solution was added with different concentrations of compound 2 (0–100 μ M) at 298, 303, and 310 K. The reaction was equilibrated for 5 min. The parameters were set as follows: the excitation wavelength was 280 nm, and the excitation and emission bandwidths were set to 5 nm. The thermodynamic parameters (ΔH and ΔS), the fluorescence quenching constant (K_{sv}), the quenching rate constant (K_q), the binding constant

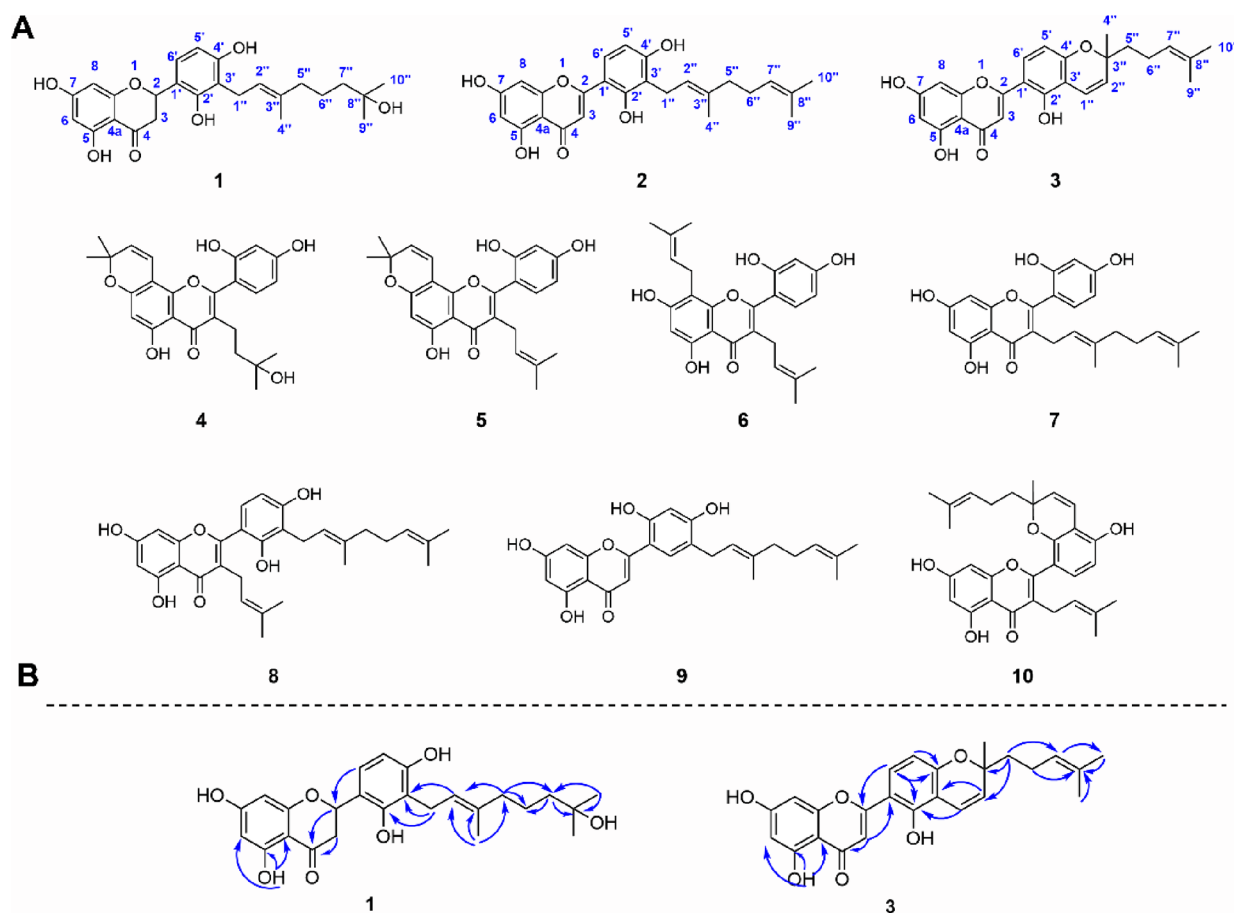


Figure 1. Structure (1–10) and carbon skeleton number of flavonoids isolated from mulberry leaves, in which compounds 1 and 3 are new compounds (A). Key HMBC correlations of compounds 1 and 3 (B).

(K_a), and the amount of fluorescence quenching binding sites (n) were calculated according to the Stern–Volmer equation, which is given below:

$$\frac{F}{F_0} = 1 + K_{SV}C_q = 1 + K_q\tau_0C_q$$

$$\log \frac{F_0 - F}{F} = \log K_a + n \log C_q$$

$$\ln K_a = -\frac{1}{T} \left(\frac{\Delta H}{R} \right) + \frac{\Delta S}{R}$$

where F_0 and F represent the presence or absence of compound 2, C_q is the concentration of compound 2, τ_0 is the lifetime of the fluorophore (10^{-8} s), and R is the gas constant of 8.31 J/(mol K).

2.7. Fourier Transform Infrared Spectroscopy. Fourier transform infrared (FTIR) spectroscopy was performed using a Thermo Nicolet iS50 FTIR spectrometer (Thermo Nicolet Corp., USA). The enzymes and flavonoids were dissolved in PBS and then lyophilized and assayed by the potassium bromide press method. The parameters were set as follows: wavelength range of 400 to 4000 cm^{-1} , resolution of 4 cm^{-1} , and 32 scans. Each spectrum was subtracted from the background air spectrum and analyzed using Thermo Scientific OMSNIC software (version 8.2, Thermo Fisher Scientific Inc., USA) and Origin software (version 9.0, Origin Lab, Co., USA).

2.8. Circular Dichroism Analysis. The determination of circular dichroism was performed with a MOS-450 circular dichroism instrument (Bio-Logic, France), and the parameters of circular dichroism were set in the wavelength range of 200–300 nm. The scanning rate was 60 nm/min, the spectral resolution was 1 nm, the response time was 1 s, and the slit width was 1 nm. Using 0.1 U/mL of

enzyme solution as the control, 12 μM compound 2 was mixed with 0.1 U/mL of α -glucosidase solution in a 1:1 volume ratio. After the addition of compound 2, the change in circular dichroism was measured. The data obtained were statistically calculated using CDPro software (Parameters Technology Corporation, USA) to analyze protein secondary structure changes including α -helices, β -folding, cornering, and random coiling.

2.9. Ultraviolet Spectroscopy Analysis. The UV–visible absorption spectra were determined using a UV–visible spectrophotometer (UV-4802, UNICO, USA) with the following parameter settings: wavelength range of 200–300 nm, slit width of 2 nm, and a standard cuvette with a path width of 1 cm. Using 0.1 U/mL of enzyme solution as control, 12 μM compound 2 was mixed with 0.1 U/mL of α -glucosidase solution in a 1:1 volume ratio. After the addition of compound 2, the change in UV–vis absorption spectra was measured.

2.10. Experimental Animals. Male C57BL/6J mice (SPF) weighing 18–20 g were purchased from the Liaoning Changsheng Biotechnology Co., Ltd. (Benxi, Liaoning, China). Mice were housed in the SPF Animal House of College of Animal Science and Veterinary Medicine, Shenyang Agricultural University under a 12 h light–dark cycle at a controlled temperature (23 ± 1 °C). During the adaptation period (1 week), the mice received a standard pellet diet and water ad libitum. All animal experiments were performed in compliance with the relevant laws and institutional guidelines for the care and use of laboratory animals in China (GB/T 35823-2018 and GB/T 35892-2018). The experiments were also reviewed and approved by the Ethical Review Committee and Laboratory Animal Welfare Committee of Shenyang Agricultural University, and the animal ethical approval number is 2023041002.

2.11. Oral Maltose Tolerance Test. The effect of mulberry leaves extracts and compound 2 on postprandial hyperglycemia was evaluated by an oral maltose tolerance test. Acarbose was dissolved in distilled

water, while mulberry leaves extracts and compound **2** were dispersed in 0.5% sodium carboxymethylcellulose solution (CMC-Na). The C57BL/6J mice were allocated to one of four groups with eight mice in each. Group 1: blank control, 0.5% CMC-Na solution was given to mice by oral gavage. Group 2: Acarbose was given to mice by oral gavage at a dose of 25 mg/kg body weight (BW). Groups 3 and 4: mulberry leaf extracts and compound **2** were given to mice by oral gavage at a dose of 25 mg/kg BW, respectively. The mice were fasted for 12 h and then received drugs by oral gavage, followed by 2 g/kg of maltose solution after 15 min. The blood glucose level was detected from the tail vein at 0, 15, 30, 60, and 120 min after maltose loading using a YUWELL glucometer (Shanghai, China). The area under the curve (AUC) over a period of 120 min was calculated based on the trapezoidal method.

2.12. Homology Modeling. The crystal structure of *Saccharomyces cerevisiae*-derived α -glucosidase has not been solved yet; therefore, different ways of homology modeling methods were used for the construction of 3D models of α -glucosidase. The primary sequence of α -glucosidase was obtained from the UniProt Protein Resource Database (<http://uniprot.org/>) with the code P53341. The PDB numbers 3A4A, 3AXH, and 3AJ7 were used as construction templates, and the protein structure was constructed by SWISS-MODEL (<https://swissmodel.expasy.org/>). At the same time, the structure in the AlphaFold Protein Structure Database (<https://alphafold.ebi.ac.uk>) was compared. Finally, the overall quality factor, Ramachandran plot, and residues in the most favored regions were used to select the best 3D structure of α -glucosidase.

2.13. Molecular Docking. The screened α -glucosidase structure was used as a receptor for molecular docking, its possible active pockets were predicted by DoGSite and FTMAP, and recommendations were given. Ten flavonoids were used as ligands for spatial conformation optimization using ChemBiodraw 3D (2019 Version) and spatial size calculation using Spartan (student edition v.9) to match the active pocket of the receptor. After comprehensive consideration of the receptor active pocket prediction and ligand space size, the combined pockets of Site1 and Site2 were selected as the molecular docking study. The molecular docking software used was Autodock Vina (v.1.5.6), and the dimensions of the active site box were set at 60 Å × 60 Å × 60 Å. Docking visualization was done using PyMOL (v.2.0) and Ligplot⁺ (v.2.2).

2.14. Molecular Dynamics. The docking results were selected as the initial structure, amber14sb was selected as the protein force field, Gaff2 was selected as the small-molecule force field, and the TIP3P model was used to add solvent to the α -glucosidase-flavonoid system, establish a water box, and add a sodium ion balance system. The PME handled the electrostatic interactions using the Verlet and cg algorithms, respectively, under elastic simulation, using the steepest descent method for energy minimization with a maximum number of steps (50,000 steps). The Coulomb force cut-off distance and van der Waals radius cut-off distance are both 1.4 nm. Finally, the canonical system (NVT) and the isothermal and isobaric system (NPT) are used to balance the system, and then the MD simulation is performed at room temperature and pressure for 100 ns. The integration step is 2 fs, and the structure is stored every 20 ps.

2.15. Compounds ADMET Characteristic Prediction. The drug-like properties of the 10 compounds, including absorption, distribution, metabolism, excretion, and toxicity (ADMET), were evaluated by use of ADMETLab 2.0 (<https://admetmesh.scbdd.com/>).

2.16. Statistical Analysis. One-way ANOVA and Tukey's tests were performed using Origin 8.5 software (OriginLab, Northampton, MA, USA) to assess significant differences ($p < 0.05$). All experiments were performed at least three times, and experimental data were presented as mean \pm SD.

3. RESULTS

3.1. Structural Elucidation of the New Compounds.

The 95% ethanol extract of the mulberry leaves were isolated by various chromatographic separation methods, including the usage of Sephadex LH-20 gel column, ODS reversed-phase

column, and silica gel column as well as semi-preparative HPLC. Two new geranylated flavonoid compounds (**1** and **3**) and their related structural analogues (**2** and **4–10**) were isolated (Figure 1).

Compound **1** was isolated as a yellow powder. The molecular formula, C₂₅H₃₀O₇, was deduced from its HR-ESI-MS data (m/z 441.1937 [M-H]⁻, calcd. 441.1913), requiring 11 degrees of unsaturation. The UV absorption band of this compound at 288 nm was suggestive of a flavanone derivative. Its IR spectrum showed the absorption band of a conjugated ketone carbonyl (1639 cm⁻¹). The ¹H NMR spectrum of **1** (Table 1) displayed

Table 1. ¹H (400 MHz) and ¹³C NMR (100 MHz) Spectroscopic Data of Compounds **1** and **3** (in Acetone-*d*₆)

position	1		3	
	δ_C	δ_H (J in Hz)	δ_C	δ_H (J in Hz)
2	76.2	5.75, (1H, dd 13.0, 2.9)	162.5	
3	42.4	2.73, (1H, dd, 17.1, 2.9) 3.20, (1H, dd, 17.1, 13.0)	109.0	7.00, (1H, s)
4	197.6		183.4	
5	165.2		163.4	
6	96.9	5.97, (1H, brs)	99.6	6.26, (1H, d, 2.0)
7	167.4		164.9	
8	96.0	5.97, (1H, brs)	94.6	6.49, (1H, d, 2.0)
9	164.4		158.9	
10	103.1		105.3	
1'	117.9		112.0	
2'	154.1		154.6	
3'	116.8		110.6	
4'	157.2		157.1	
5'	108.3	6.55, (1H, d, 8.4)	109.4	6.64, (1H, d, 8.8)
6'	125.7	7.14, (1H, d, 8.4)	129.8	7.71, (1H, d, 8.8)
1''	23.0	3.47, (2H, d, 6.9)	117.9	6.79, (1H, d, 10.1)
2''	123.4	5.28, (1H, t, 6.9)	128.7	5.77, (1H, d, 10.1)
3''	136.0		81.0	
4''	16.3	1.79 (3H, s)	26.7	1.50 (3H, s)
5''	40.9	1.97, (2H, t, 6.8)	41.9	1.81, (2H, m)
6''	23.3	1.49, (2H, m)	23.6	2.17, (2H, m)
7''	44.1	1.42, (2H, m)	124.8	5.12, (1H, t, 7.2)
8''	70.8		132.4	
9''	29.5	1.17 (3H, s)	25.8	1.61 (3H, s)
10''	29.5	1.17 (3H, s)	17.7	1.52 (3H, s)
5-OH		12.20, brs		13.06, brs

signals due to a chelate hydroxyl group at δ_H 12.20 (1H, brs, OH-5), a pair of *ortho*-coupled aromatic protons at δ_H 6.55 (1H, d, $J = 8.4$ Hz, H-5') and 7.14 (1H, d, $J = 8.4$ Hz, H-6'), and a set of typical *meta*-coupled aromatic protons [δ_H 5.97 (2H, s, H-6 and H-8)] (Table 1). In addition, the characteristic signals of an oxymethylene proton at δ 5.75 (dd, $J = 13.0, 2.9$ Hz, H-2) and a methylene unit at δ_H 2.73 (dd, $J = 17.1, 2.9$ Hz, Ha-3) and 3.20 (dd, $J = 17.1, 13.0$ Hz, Hb-3) were also observed. **1** was established to possess a flavanone skeleton in conjunction with the appearance of one oxygenated carbon signals at δ_C 76.2 (C-2).

Moreover, the characteristic signals of **1** at δ_H 5.28 (1H, t, $J = 6.9$ Hz, H-2''), 3.47 (2H, d, $J = 6.9$ Hz, H-1''), 1.97 (2H, t, $J = 6.8$ Hz, H-5''), 1.79 (3H, s, H-4''), 1.49 (2H, m, H-6''), 1.42 (2H, m, H-7''), and 1.17 (6H, s, H-9'', H-10''), together with the typical carbon signals at δ_C 70.8 (C-8'') implied the presence of a 7-hydroxy-3,7-dimethyl-2(*E*)-octenyl group (hydroxylated geranyl).¹⁶ Due to the increased γ -gauche effect, the geometry of

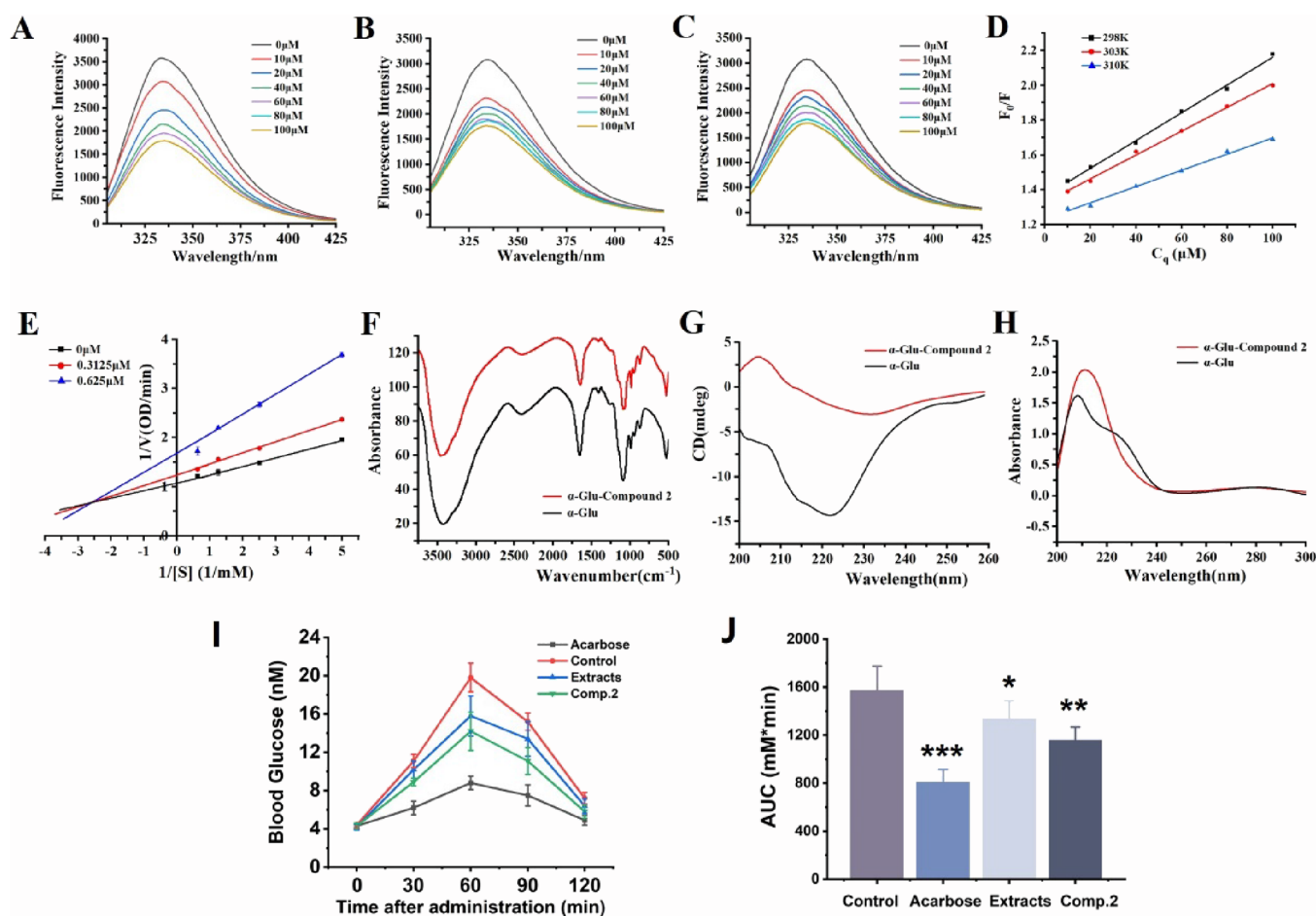


Figure 2. Inhibition mechanism of compound 2 against α -glucosidase. (A) Fluorescence spectrum of compound 2 with α -glucosidase at 298 K. (B) Fluorescence spectrum of compound 2 with α -glucosidase at 303 K. (C) Fluorescence spectrum of compound 2 with α -glucosidase at 310 K. (D) Stern–Volmer plots of α -glucosidase with the addition of compound 2 at different temperatures. (E) Lineweaver–Burk plot of compound 2. (F) FT–IR spectra of α -glucosidase treated with compound 2. (G) CD spectra of α -glucosidase treated with compound 2. (H) UV spectra of α -glucosidase treated with compound 2. (I) Blood glucose concentrations after oral administration of flavonoids and maltose. (J) Area under the curve (AUC) after oral administration of flavonoids and maltose for 2 h.

the C-2''/C-3'' double bond was attributed to be an *E* form on the basis of an upfield chemical shift of the methyl carbon C-4'' at δ_C 16.3. The ^{13}C -NMR data of **1** showed 25 signals including two benzene rings, a ketone group, and a hydroxylated geranyl group. A comparison of the ^1H and ^{13}C NMR spectral data of **1** (Table 1) with sanggenol A¹⁷ indicated that they are structural analogues, but the major difference is the appearance of a hydroxyl group at C-8'' (δ_C 70.8), implying that **1** was a hydroxylated derivative of sanggenol A.

The long-range correlations further verified the existence of 7-hydroxy-3,7-dimethyl-2(*E*)-octenyl moiety in **1** (Figure 2). The long-range correlations of H-1'' at δ_H 3.47 with C-3' (δ_C 116.8), C-2' (δ_C 154.1), and C-4' (δ_C 157.2), and H-2'' at δ_H 5.28 with C-3' in the HMBC spectrum confirmed that the unequivocal assignment of the hydroxylated geranyl group at C-3' position. The planar structure of **1** could be established based on the information mentioned above. The absolute configuration at C-2 of **1** was elucidated as *S* based on the negative cotton effect observed at 292 nm in the ECD spectrum.¹⁸ Accordingly, **1** was determined as 2*S*-3'-(2*E*)-7-hydroxy-3,7-dimethyl-2-octen-1-yl-2',4',5,7-tetrahydroxyflavone and named as mortatarin F.

Compound **3** was isolated as a yellow amorphous powder. Its molecular formula was assigned as $\text{C}_{25}\text{H}_{24}\text{O}_6$ based on the HR-ESI-MS (m/z 421.1621 [$\text{M} + \text{H}$]⁺, calcd. 421.1651) with 14

degrees of unsaturation. The UV spectrum of this compound, with absorption maxima at 266 and 352 nm, was indicative of a flavonoid skeleton. Its IR spectrum indicated the presence of a conjugated carbonyl group (1648 cm^{-1}) and a hydroxyl group (3381 cm^{-1}). Examination of the NMR spectra data for compound **3** suggested a close similarity to compound **2**, in addition to the existence of the pyran ring signals and the absence of the prenyl moiety signals. Thus, we can speculate that compound **3** could be biosynthesized in the plant from the precursor **2** based on cyclization of the geranyl side chain with the adjacent phenolic hydroxyl group at C-4'.

The HMBC experiment further confirmed the position of the pyran ring (Figure 2). The HMBC correlations of H-2'' (δ_H 5.77) with C-3' (δ_C 110.6) and of H-1'' (δ_H 6.79) with C-3' (δ_C 110.6), C-2' (δ_C 154.6), and C-4' (δ_C 157.1) demonstrated that the pyran ring was fused to C-3'/4' of the flavone skeleton with an ether linkage at C-4'.

The computation of ECD data using time-dependent density functional theory (TDDFT) was used to determine the absolute configuration of the C-3'' of **3**. Since compound **3** must be one of the two enantiomers (3''*R*)-**3** (**3a**) or (3''*S*)-**3** (**3b**) based on the planar structure analysis, the two enantiomers were differentiated by the ECD method. However, we found that the experimental ECD curve of **3** can not match well with the

calculated curve of (3''R or 3''S)-3. (Figure S16). Moreover, compound 3 showed a very small specific rotation, $[\alpha]_D^{25}$ -2.8 (c 0.2, MeOH), implying that this compound should be a scalemic mixture. Unfortunately, compound 3 could not be further resolved via a chiral HPLC column due to the small amount of compound remaining. Therefore, the structure of 3 was established and named as mortatarin G.

The structures of the known compounds sanggenon W (2),¹⁹ morusinol (4),²⁰ morusin (5),²¹ kuwanon C(6),²² 5,7,2',4'-tetrahydroxy-3-geranylflavone (7),²³ 3'-geranyl-3-prenyl-2',4',5,7-tetrahydroxyflavone (8),⁹ 5'-geranyl-5,7,2',4'-tetrahydroxyflavone (9),²⁴ and sanggenone K (10)²⁵ were elucidated by comparison of their spectroscopic data with those of the reported literature. Meanwhile, compounds 7 and 9 were purified from mulberry leaves for the first time. In this work, two new compounds were separated from the leaves, and their structures were identified, which would be helpful to enrich and understand the chemical components of mulberry leaves.

3.2. Summary of the Structural Information of the Novel Prenylated Flavonoids. Mortatarin F (1): yellow amorphous powder (MeOH); UV (MeOH) λ_{\max} (log ϵ) 288 (3.81) nm; IR (KBr) ν_{\max} 3375, 2927, 1639, 1605, 1500, 1459, 1345, 1300, 1161, 1020, 809 cm^{-1} ; ¹H and ¹³C NMR data: see Table 1; HRESIMS m/z : 441.1937 [M-H]⁻ (calcd. for C₂₅H₂₉O₇, 441.1913).

Mortatarin G (3): yellow amorphous powder (MeOH); $[\alpha]_D^{25}$ -2.8 (c 0.2, MeOH); UV (MeOH) λ_{\max} (log ϵ) 266 (4.36) and 352 (4.12) nm; IR (KBr) ν_{\max} 3381, 2970, 1648, 16134, 1566, 1439, 1353, 1303, 1247, 1164, 814 cm^{-1} ; ¹H and ¹³C NMR data: see Table 1; HRESIMS m/z : 421.1621 [M + H]⁺ (calcd. for C₂₅H₂₅O₆, 421.1651).

3.3. α -Glucosidase Activity and Molecular Docking Analysis. In order to verify the potential regulatory ability of flavonoids separated from mulberry leaves on postprandial blood glucose, 10 compounds were detected by α -glucosidase inhibition test.²⁶ The results showed (Table S1) that the IC₅₀ range of the compound's inhibitory activity on α -glucosidase was 2.6–22.6 μM , which was similar to the positive drug acarbose (IC₅₀ = 19.6 μM). The molecular docking scoring evaluation was further carried out using the constructed 3D structure of α -glucosidase, and it was found that the scoring range of compounds 1–10 was between -9.2 and -10.6 kcal/mol, and the scoring value of acarbose was -8.7 kcal/mol. Both the inhibition test and molecular docking showed that compounds 1–10 had good inhibitory activity *in vitro*. Considering comprehensively, we selected compound 2 with relatively good activity for the in-depth study of its molecular mechanisms.

The enzyme kinetics type of α -glucosidase inhibition by compound 2 was analyzed using Lineweaver–Burk double inverse plotting. The results (Figure 2E) showed that the three straight lines at different inhibitor concentrations intersected in the second quadrant of the coordinate axis, which indicated that the maximum reaction rate V_{\max} of the enzymatic reaction decreased with increasing compound 2 concentration and the K_m values changed accordingly. Lineweaver–Burk analysis showed that compound 2 is a mixed inhibitor of α -glucosidase.

3.4. Multispectroscopic Analysis of the Mechanism of Inhibition. Three fluorescent chromophores, Trp, Tyr, and Phe, are included in the proteins, and when their fluorescence peaks and fluorescence signals change, they can reflect the interactions that occur with the substances.²⁷ α -Glucosidase had a strong fluorescence emission peak at 335 nm, and the

fluorescence intensity decreased gradually with the addition of compound 2 (Figure 2A–C), indicating that the compound interacted with the glucosidase. The quenching at different temperatures was then investigated, and it was found that the K_{sv} values all decreased with increasing temperature. The quenching rate constants (K_q) at 298, 303, and 310 K were 8.12×10^{11} , 7.09×10^{11} , and 4.51×10^{11} L/mol s, respectively, which were higher than the maximum biomolecular collision quenching constant (2×10^{10} L/mol s). These results indicate that static quenching dominates the fluorescence quenching process. The number of binding sites (n) was close to 1 at all three temperatures, and the value gradually decreased with increasing reaction temperature, inferring that compound 2 has only one binding site in α -glucosidase. The binding constants (K_a) at the three temperatures were about 10^5 L mol⁻¹ and indicated that compound 2 has a high binding affinity for α -glucosidase. Thermodynamic parameters were calculated using the Stern–Volmer equation to characterize the interaction forces between the compounds and α -glucosidase (Table S2). The calculated $\Delta G < 0$ indicates that the binding process to form the complexes proceeds spontaneously at different temperatures. Furthermore, $\Delta H < 0$ and $\Delta S < 0$ indicate that the compound binds to α -glucosidase mainly through hydrogen bonding and van der Waals force interactions (Figures S17 and S18).²⁸

The FTIR spectrum range of 1700 to 1600 cm^{-1} was used to explore the changes in secondary structure of α -glucosidase after treatment with compound 2 (Figure 2F). Upon addition of compound 2, the amide I band of α -glucosidase shifted from 1649 to 1642 cm^{-1} , indicating that compound 2 interacted with the C=O group of α -glucosidase.²⁹ In turn, rearrangement of the internal polypeptide occurred, changing the carbonyl hydrogen bond and, eventually, the secondary structure of α -glucosidase.

The results of circular dichroism were shown in Figure 2G. The circular dichroism chromatogram of α -glucosidase showed two negative cotton effects at 212 and 222 nm for the characteristic bands of the α -helix, and the characteristic peaks were due to the $n \rightarrow \pi^*$ and $\pi \rightarrow \pi^*$ electron transfer of the peptide bond.³⁰ The results showed that the α -helix content decreased from 36.2 to 28.4%, β -folding decreased from 49 to 41.4%, β -turning decreased from 22.9 to 21.7%, and irregular curling increased from 25.2 to 33.3% after the binding of compound 2 with α -glucosidase. These changes may be due to the expansion of the glycosidase polypeptide chain when compound 2 binds to the amino acid residues of α -glucosidase, resulting in the loss of the protein hydrogen bond network structure. Thus, the secondary structure of α -glucosidase was altered and the interaction between the two occurred, further affecting the activity of α -glucosidase.

With the addition of compound 2, the UV–vis absorption spectrum of α -glucosidase changed as shown in the figure (Figure 2H). α -Glucosidase had a characteristic absorption peak at 208 nm in the range of 200–300 nm, and after the addition of compound 2, the absorption peak moved from 208 to 211 nm, and the absorption peak was enhanced and redshifted. This indicates that static quenching of α -glucosidase occurs when mixed with compound 2, causing structural changes in the protein and again demonstrating that α -glucosidase interacts with compound 2.

3.5. *In Vivo* Assay of Postprandial Glucose. The *in vivo* α -glucosidase inhibitory activity of flavonoids was further evaluated by an oral maltose tolerance test in a normal mouse model. Acarbose was selected as a positive control. As we shown

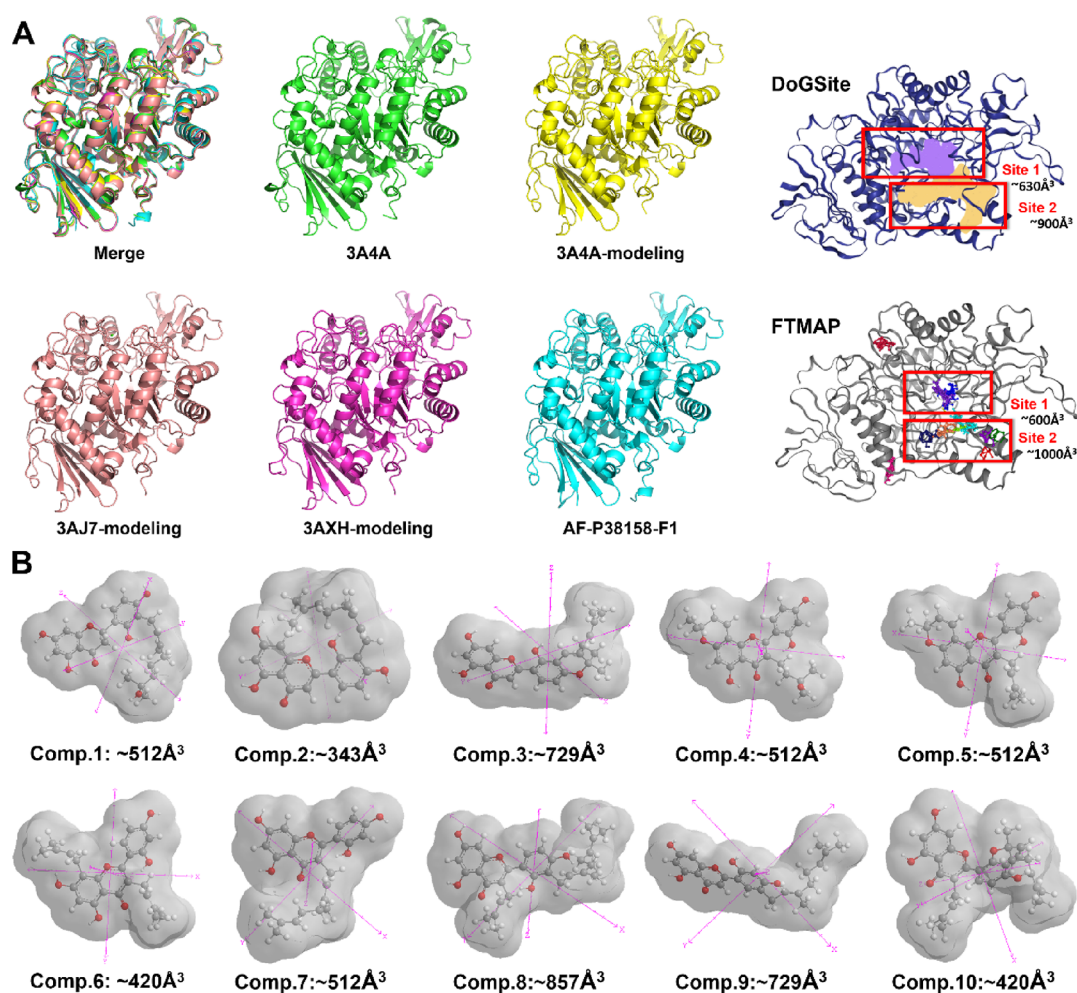


Figure 3. 3D structural diagram of α -glycosidase and mulberry leaf compounds. (A) Structure of *S. cerevisiae* derived α -glycosidase constructed with different templates and possible activity pockets prediction in AF-P38158-F1. (B) 3D structure and spatial volume of compounds 1–10.

in Figure 2I, the postprandial blood glucose level of the control group was increased rapidly and peaked at 60 min. The maximum blood glucose concentration reached to 19.8 ± 1.5 mM. In comparison to the control group, oral administration of the extracts and compound 2 significantly decreased the postprandial blood glucose level at 60 min and resulted in the decrease of $AUC_{0-120 \text{ min}}$ by 15.24 and 26.43%, respectively (Figure 2J). All these suggest that compound 2 also has good hypoglycemic ability *in vivo*.

3.6. Modeling of α -Glucosidase. Structural comparison was carried out by homology modeling, AlphaFold modeling, and 3A4A commonly used in the literature.^{31,32} The results showed that the structures of several α -glucosidase based on 3A4A modeling, 3AXH modeling, 3AJ7 modeling, AlphaFold modeling, and commonly used 3A4A were very similar (Figure 3A), and the 3D diagrams of the five structures were close to the coincidence state. Therefore, the overall quality factor, Ramachandran plot, and residues in the most favored regions were used to further evaluate the differences in the structure of the constructed α -glucosidase (Table S2). It was found that the 3D structure codenamed AF-P38158-F1 constructed based on AlphaFold was the best in all three evaluations. Therefore, the 3D structure of AF-P38158-F1 was selected as the basis for subsequent molecular docking and molecular dynamics studies. After selecting the acceptor structure, it is necessary to further determine its possible active pocket. Through the quantum

chemical calculation of 10 compounds, it can be seen that their spatial sizes vary greatly (343–857 Å). Therefore, we evaluated the modeled α -glucosidase activity pockets and found that the pockets predicted by DoGSite and FTMAP are almost the same, with two pockets of different sizes (600–1000 Å). In order to satisfy the accurate binding of ligand and receptor as much as possible, we combined the two pockets as a research area for further molecular docking and molecular dynamics.

3.7. MD Simulation Details Analysis. In molecular simulation, RMSD is used to quantify the degree of conformational difference or the degree of trajectory stability in order to rapidly determine if a given trajectory has reached equilibrium for further simulation or analysis.³³ Figure 4A showed that the RMSD of both systems fluctuated first and then stabilized. The acarbose system began to equilibrate at about 50 ns, and the compound 2 system fluctuated at about 33 ns/62 ns. Generally speaking, the fluctuations of the two systems were stable within the range of 0.1 nm, revealing good binding stability.

The RMSF calculates the fluctuation (range of change) of each atom relative to its average position, which is an indicator of the degree of freedom of atomic motion and characterizes the flexibility of the molecular structure.³⁴ Figure 4B showed that the fluctuations of the two systems are very similar, which proves that the protein system maintains a certain rigidity under the action of different small molecules without major changes.

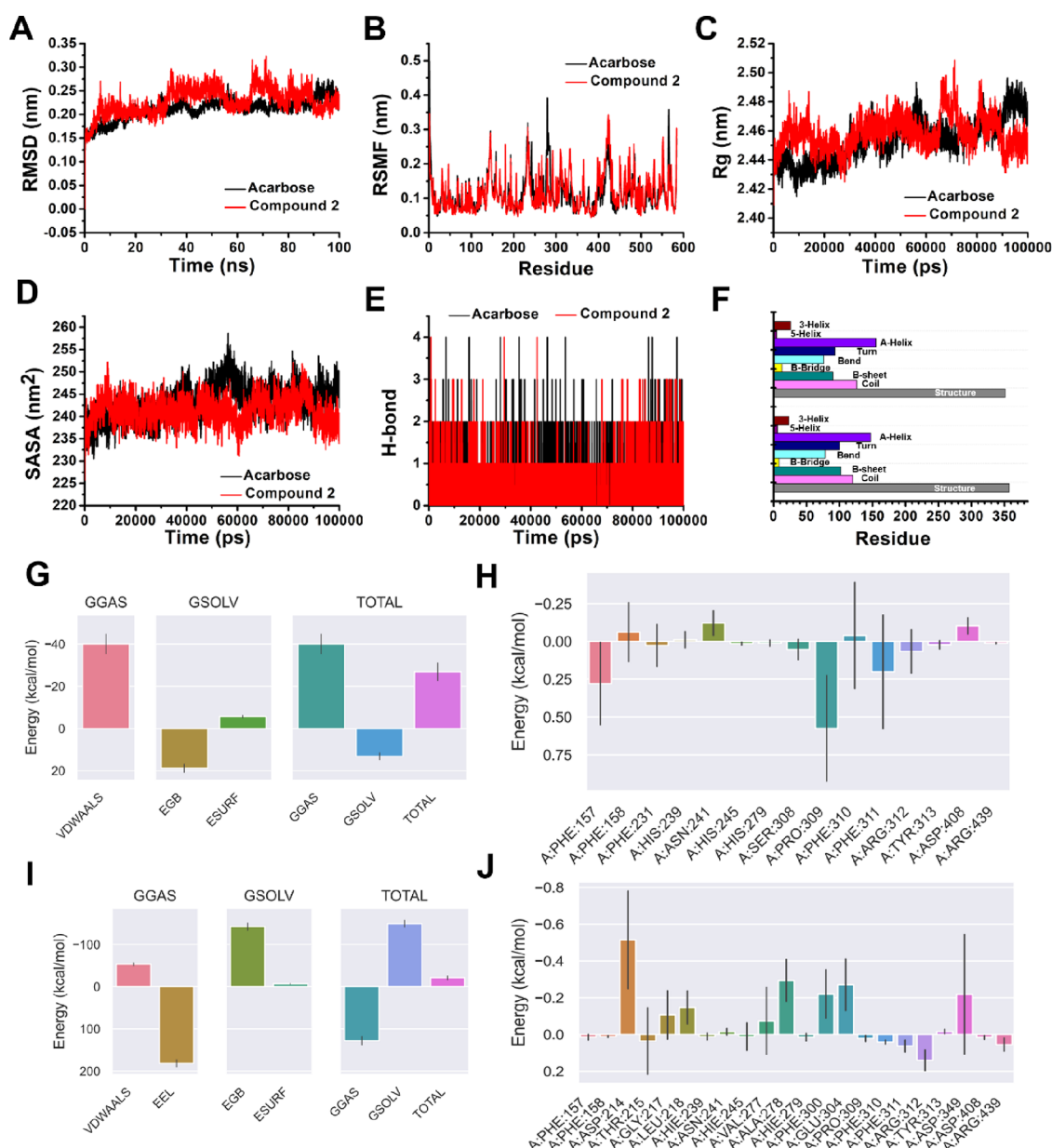


Figure 4. Molecular dynamics results of acarbose/compound 2 with α -glycosidase (AF-P38158-F1) (100 ns). (A) Root mean square deviations (RMSD, nm) of complex with acarbose/compound 2 and α -glycosidase. (B) Root mean square fluctuation (RMSF) of the complex. (C) Radii of gyration (R_g) and (D) Solvent-accessible surface area (SASA) values. (E) Hydrogen bonding of the complex. (F) Dictionary of Protein Secondary Structure (DSSP). Energy contribution analysis of different complex ((G) for acarbose, (I) for compound 2) and residue contribution analysis ((H) for acarbose, (J) for compound 2).

R_g describes the distribution of atoms in a system along a specific axis and can be used to characterize the compactness of molecules.³⁵ For example, it can be used to distinguish folded-helix structures from stretched structures or to examine the characteristic motion of a system. Changes in R_g values can represent changes in protein tertiary structure. Figure 4C showed that the calculation results of R_g are similar to the fluctuation results of RMSD. As the simulation progresses, the R_g of both systems increases and then tends to be stable, which can mutually verify the correctness of the calculation. The acarbose/ α -glycosidase system fluctuated around 50 ns and then stabilized. The compound 2/ α -glycosidase system fluctuated at about 70 ns and then gradually stabilized.

SASA can study protein folding stability, determine the surface area after interaction between proteins and small

molecules, and predict the structural free energy between ligands and receptors.³⁶ Figure 4D shows that the compound 2/ α -glycosidase system first increased and then decreased while the acarbose/ α -glycosidase system increased, indicating that under the action of small molecules, the protein pocket of the acarbose system slightly increased a little, so the surface area becomes larger. Hydrogen bonding is the most important non-covalent structural force (mainly electrostatic in nature) in molecular systems. Figure 4E showed that in the dynamic process from 0 to 100 ns, the hydrogen bonding interactions of the two systems alternate with each other and there is no obvious difference between the two.

DSSP is a standardized algorithm for secondary structure conformation classification of amino acid residues in protein structures. Figure 4F showed that the combination of acarbose

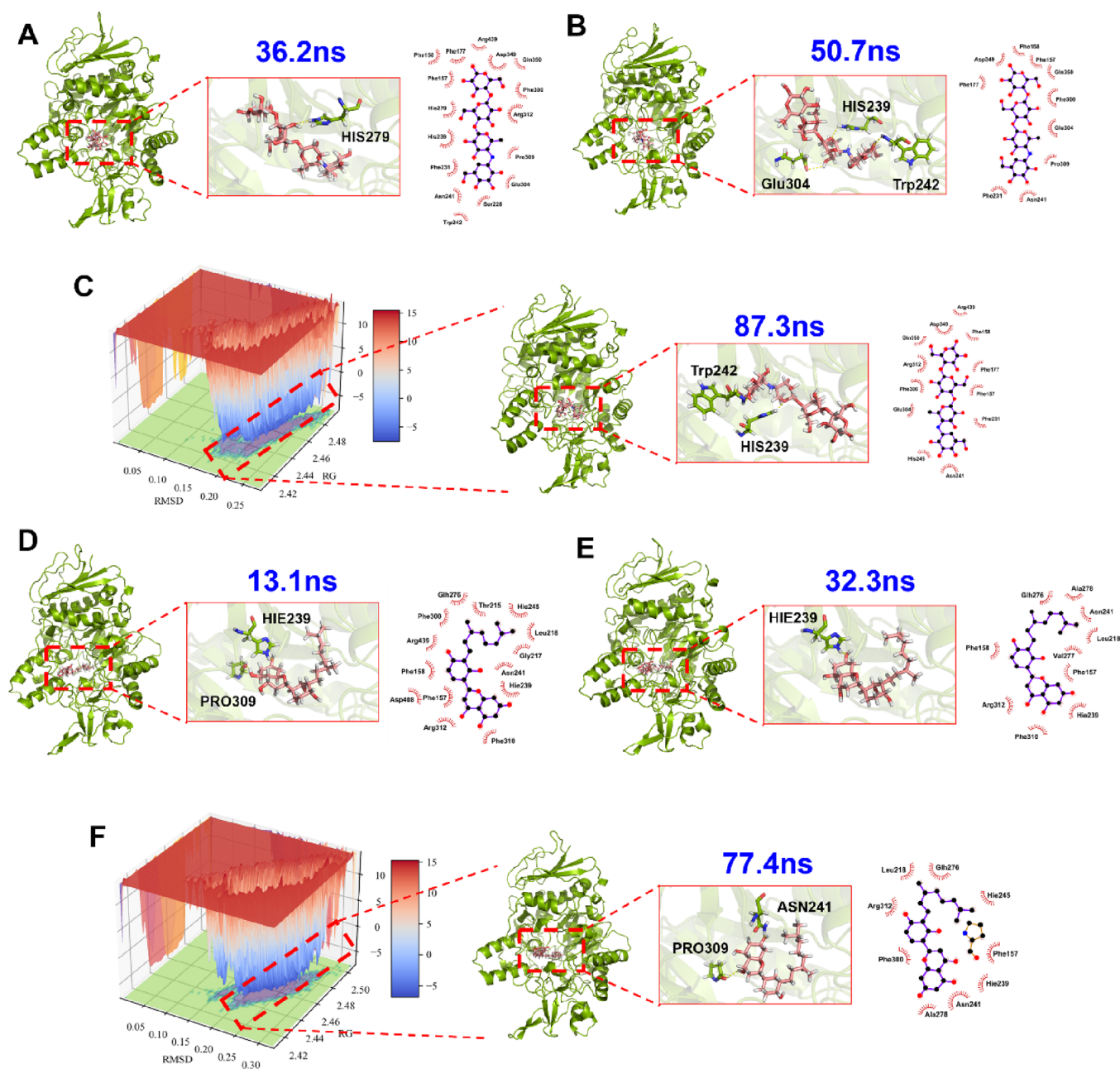


Figure 5. Free energy landscapes and lowest energy conformation comparison. (A, B) Schematic diagrams of the timepoint interaction of acarbose and α -glucosidase complexes during the molecular dynamics process of obvious conformational changes. (C) Schematic diagram of the interaction of the optimal steady-state conformation. (D, E) Schematic diagrams of the timepoint interaction between compound 2 and the α -glucosidase complex during the molecular dynamics process of obvious conformational changes. (F) is a schematic diagram of the interaction of the optimal steady-state conformation.

and α -glucosidase results in more coil curling, less β -sheet, more β -bridge, more α -helix, and less 3-helix. Compound 2 binds to α -glucosidase with less coil curling, less β -sheet, more β -bridge, more α -helix, and less 3-helix.

The structure after 100 ns equilibrium was calculated, and the interaction energy contribution of acarbose and compound 2 with α -glucosidase was analyzed. Figure 4G showed that after acarbose and glycosidase are combined, the contribution of G_{gas} mainly comes from van der Waals forces, and the contribution of G_{solv} mainly comes from EGB and ESURF. In general, van der Waals force plays a major role. The calculated binding free energy is decomposed into the contribution of each atom, and then the atomic contributions are added according to groups to

obtain the contribution of residues, residue skeletons, or residue side chains to the binding free energy, and the contribution values of different residues to the combination of the two are obtained (Figure 4H,J). The results showed that the residues involved in the binding of compound 2 and acarbose to α -glucosidase were similar but the contribution was significantly different, which was consistent with the molecular docking and other molecular dynamics parameters mentioned above.

3.8. Dynamic Binding Process Analysis. For the hydrogen bonding of the acarbose/ α -glucosidase system, at 36.2 ns, the molecular structure of acarbose was partially reversed under the action of HIS-279 residue (Figure 5A). At 50.7 ns, the whole small molecule left HIS-279, and its structure

completed a lateral turnover, interacting with HIS-239, TRP-242, and GLU-304 (Figure 5B). At 87.3 ns, acarbose gradually stabilized after lateral overturning and linked to HIS-239 and TRP-242.

For the hydrogen bonding of the compound 2/ α -glucosidase system, the conformation of the small-molecule B ring was at 13.1 ns and gradually moved up, forming hydrogen bonds with HIE-239 and PRO-309. At 32.3 ns, the tail side-chain structure of compound 2 sinks, leaving only the interaction between the head B-ring and HIE-239. At 77.4 ns, the B-ring of compound 2 also began to sink, leaving only the interaction relationship with PRO-309, while the residue originally interacting with HIE-239 changed to ASN-241.

Similarly, the interaction residues in the non-hydrogen bond system also changed significantly. In the acarbose/ α -glucosidase system, the main residues involved at 36.2 ns were Phe157/Phe158/Phe177/Ser288/Trp242/Asn241/Phe231/His239/His279/Glu304/Pro309/Arg312/Phe300/Gln350/Asp349/Arg439. The main involved residues at 50.7 ns were Phe157/Phe158/Phe177/Phe231/Asn241/Phe300/Glu304/Pro309/Asp349/Gln350. The main involved residues at 87.3 ns were Phe157/Phe158/Phe177/Phe231/Asn241/His245/Phe300/Glu304/Arg312/Asp349/Gln350/Arg439. In the compound 2/ α -glucosidase system, the main residues involved at 13.1 ns were Phe157/Phe158/Thr215/Gly217/Leu218/His239/Asn241/Gln276/Phe300/Phe310/Arg312/Asp408/Arg439. The main involved residues at 32.3 ns were Phe157/Phe158/Leu218/His239/Asn241/Gln276/Val277/Ala278/Phe310/Arg312. The main involved residues at 77.4 ns were Phe157/Leu218/His239/Asn241/His245/Gln276/Ala278/Phe300/Arg312.

3.9. ADMET Characteristic Prediction. ADMET is an important reference indicator for whether a compound has potential application value.³⁷ Therefore, this study evaluated the basic properties of compounds 1–10 by means of network prediction, including: MW/nRing/FChar/nHet/MaxRing/nRing/nRot/TPSA/nHD/nHA/LogD/LogS/LogP. It can be seen from the radar chart of the results (Figure S19) that the properties of the compounds are relatively consistent, which is similar to the α -glucosidase inhibition tests and the molecular docking score, indicating that this type of prenylated flavonoid in mulberry leaves has similar structural activity and ADMET properties.

4. DISCUSSION

Mulberry leaves are highly popular as a dual-purpose plant for medicine and food with a long history of use.¹⁰ However, the previous studies on the chemical components of mulberry leaves mainly focused on the flavonoid aglycones with simple substituents and their glycosides (glycosylation, methylation, etc.),¹¹ and there were few studies on flavonoids with prenylated substitution. Based on the previous discovery of prenylated flavonoids in mulberry leaves,¹⁴ this study further investigated their chemical composition and further found 10 characteristic prenylated flavonoids, of which compounds 1 and 3 were new compounds and compounds 7 and 9 were found in mulberry leaves for the first time. The above research results enrich the chemical composition of mulberry leaves, and combined with the previous research results, we can preliminarily infer that prenylated flavonoids in mulberry leaves are of great significance to their chemical composition.

Chemical components are often directly related to functionality.^{38,39} At present, studies have confirmed that the main contributor to the hypoglycemic activity of mulberry leaves is

flavonoids, especially simple substituent flavonoids.^{8,10} There are few reports on the hypoglycemic activity of prenylated flavonoids in mulberry leaves, but from the perspective of chemical structure, prenylated flavonoids have clear glycosidase inhibitory activity. For example, three prenylated flavonoids isolated from *Derris scandens Benth* and seven prenylated flavonoids found from *Dorstenia psilurus*⁴⁰ showed different degrees of α -glucosidase inhibition effect. This study also found that prenylated flavonoids in mulberry leaves have good α -glucosidase inhibitory activity, which further explains the potential contribution of complex substituted flavonoids in mulberry leaves to the regulation of blood glucose based on chemical substances. Accordingly, it was meaningful and valuable to summarize the contribution of substituents to glycosidase inhibitory activity and infer the preliminary structure–activity relationship based on the experimental data. The isolated compounds possessed the same flavonoid skeleton (5,7,2',4'-tetrahydroxyflavone) except for major differences in the prenylation substitution positions and patterns. Compound 2 exhibited better α -glucosidase inhibitory activity than 7 and 9, indicating that the geranyl substituted on C-3' of C ring of the flavone nucleus can enhance the hypoglycemic activity. The hydroxylation (1) or cyclization to pyran ring (3) of the geranyl group lowered the activity in comparison to 2, suggesting that the hydrophobic unsaturated acyclic geranyl group may be crucial for the hypoglycemic activity. Moreover, the presence of an additional prenyl group substituted on C-3 of the flavone skeleton reduced the activity (2 versus 8 and 3 versus 10). In addition, the glycosidase inhibitory activity of compounds 4 and 5 was more potent than that of the corresponding compound 6, which possess an unsaturated prenyl, revealing that the activity increased with the rise of polarity of the prenyl group.

Molecular docking and molecular dynamics are effective methods to study the interaction between different molecules through computational simulation, which are widely used in biomedicine, food, chemistry, and other fields.⁴¹ The inhibitory effects of ligands and receptors can be mutually verified by molecular docking and molecular dynamics. First of all, we need to have a clear structure of the macromolecular receptor and small-molecule ligand. The structure of the small-molecule ligand is generally easy to obtain, while the structure of the macromolecular receptor often highly depends on the structural information of the PDB data.^{42,43} If there is no clear PDB molecular structure, it needs to be simulated. It is worth noting that the current sources of α -glucosidase used in *in vitro* experiments are all *S. cerevisiae* sources, and *S. cerevisiae*-derived α -glucosidases have no PDB structure.⁴⁴ At this stage, there are various protein structures used in the research on α -glucosidase, such as the use of *S. cerevisiae* isomaltase with PDB numbers 3A4A, 3AXH, and 3AJ7 as the construction template for molecular docking research.^{30,44} Therefore, the question of which structure is more accurate for molecular simulation studies must be considered. This study compared the structure of the protein constructed with 3A4A, 3AXH, and 3AJ7 and the AF-P38158-F1 protein structure modeled by the current high-accuracy AlphaFold model. Through multi-index analysis, it was found that AF-P38158-F1 has the best structural score, and its protein structure can be downloaded from the website for free. It is the best model protein before the crystal structure of *S. cerevisiae*-derived α -glucosidase is obtained. It is recommended for follow-up research.

After selecting the model protein, this study carried out molecular docking and molecular dynamics studies on

compound **2** and the positive drug acarbose. From the results, the information given by molecular docking is slightly different from that of molecular dynamics, and most of the current studies are based on molecular docking results for analysis and discussion, which may miss or lose key missing information.⁴⁵ For example, the interaction residues and chemical bonds of compound **2** and acarbose in this study are quite different, and compound **2** should not have good activity only from the static point of view of molecular docking. However, the RMSD, RMSF, SASA, Rg, and other information provided by the dynamic analysis of molecular dynamics played an important role. Similarly, Wang et al. research also proved that MD is more accurate for the study of α -glucosidase inhibitory activity.³³ The binding of small molecules to proteins is usually maintained by four molecular forces, including van der Waals forces, electrostatic forces, hydrophobic interactions, and hydrogen bonds. Based on Ross and Subramanian's theory (namely, relative values' change in enthalpy and entropy), the main molecular forces in the binding process can be inferred.²⁷ The calculated $\Delta G < 0$ indicates that the binding process to form the complexes proceeds spontaneously. Furthermore, $\Delta H < 0$ and $\Delta S < 0$ indicate that the compound binds to α -glucosidase mainly through hydrogen bonding and van der Waals force interactions. The above spectroscopic experiments are in general agreement with the results of molecular docking and molecular dynamics experiments. That is, van der Waals forces drive the interaction between the two, with hydrogen bonding and electrostatic forces playing a secondary role.

All in all, 10 characteristic prenylated flavonoids were isolated from mulberry leaves in this study, among which compounds **1** and **3** were new compounds, and **7** and **9** were found in mulberry leaves for the first time. *In vitro* α -glucosidase inhibition test showed that all compounds showed good activities with mixed inhibition types. Meanwhile, it is proven that in addition to common flavonoids, the characteristic prenylated flavonoids are also an important chemical basis for mulberry leaves to regulate blood glucose. Through the multi-spectroscopic method, molecular docking, and molecular dynamics studies, it was found that prenylated flavonoids (represented by compound **2**) had a mixed inhibition effect of α -glucosidase and the binding process was spontaneous with van der Waals forces, hydrogen bonding, and electrostatic forces. At the same time, the ADMET prediction of the 10 compounds showed that the prenylated flavonoids from mulberry leaves all had good bioabsorption properties. The above research provides an important theoretical basis for the hypoglycemic application of prenylated flavonoids from mulberry leaves.

■ ASSOCIATED CONTENT

SI Supporting Information

The Supporting Information is available free of charge at <https://pubs.acs.org/doi/10.1021/acs.jafc.3c00776>.

(Figures S1 – S19) Characterization data of the new compounds: UV, IR, CD, ¹H, ¹³C, 2D NMR, and HRESIMS spectra, molecular docking map, and spider web plot of the properties predicted by the online prediction tool ADMETLab 2.0; (Table S1) α -glucosidase inhibitory activities of isolated compounds **1–10**; (Table S2) binding process parameters (K_d , K_a , ΔS , ΔH , and ΔG) between compound **2** and α -glucosidase; (Table S3) information of α -glucosidase constructed by different templates; (Scheme S1)

extraction and isolation procedure of mulberry leaves (PDF)

■ AUTHOR INFORMATION

Corresponding Authors

Sheng-Li Niu – Key Laboratory of Livestock Infectious Diseases, Ministry of Education, Key Laboratory of Ruminant Infectious Disease Prevention and Control (East), Ministry of Agriculture and Rural Affairs, College of Animal Science and Veterinary Medicine and College of Food Science, National R&D Professional Center For Berry Processing, National Engineering and Technology of Research Center For Small berry, Key Laboratory of Healthy Food Nutrition and Innovative Manufacturing, Liaoning Province, Shenyang Agricultural University, Shenyang, Liaoning 110866, China; Email: niushengli@syau.edu.cn

Ping Hu – Key Laboratory of Research on Pathogenesis of Allergen Provoked Allergic Disease in Liaoning Province, Shenyang Medical College, Shenyang 110034, China; Email: huping1277@163.com

Authors

Jin-Long Tian – College of Food Science, National R&D Professional Center For Berry Processing, National Engineering and Technology of Research Center For Small berry, Key Laboratory of Healthy Food Nutrition and Innovative Manufacturing, Liaoning Province, Shenyang Agricultural University, Shenyang, Liaoning 110866, China; orcid.org/0000-0001-7149-9441

Min Zhao – College of Food Science, National R&D Professional Center For Berry Processing, National Engineering and Technology of Research Center For Small berry, Key Laboratory of Healthy Food Nutrition and Innovative Manufacturing, Liaoning Province, Shenyang Agricultural University, Shenyang, Liaoning 110866, China; orcid.org/0000-0002-6350-9053

Jing-Yi Xu – Key Laboratory of Livestock Infectious Diseases, Ministry of Education, Key Laboratory of Ruminant Infectious Disease Prevention and Control (East), Ministry of Agriculture and Rural Affairs, College of Animal Science and Veterinary Medicine, Shenyang Agricultural University, Shenyang, Liaoning 110866, China

Tian-Meng Lv – Key Laboratory of Livestock Infectious Diseases, Ministry of Education, Key Laboratory of Ruminant Infectious Disease Prevention and Control (East), Ministry of Agriculture and Rural Affairs, College of Animal Science and Veterinary Medicine, Shenyang Agricultural University, Shenyang, Liaoning 110866, China

Xiao-Chang Liu – Key Laboratory of Research on Pathogenesis of Allergen Provoked Allergic Disease in Liaoning Province, Shenyang Medical College, Shenyang 110034, China

Sheng Sun – Key Laboratory of Livestock Infectious Diseases, Ministry of Education, Key Laboratory of Ruminant Infectious Disease Prevention and Control (East), Ministry of Agriculture and Rural Affairs, College of Animal Science and Veterinary Medicine, Shenyang Agricultural University, Shenyang, Liaoning 110866, China

Qi Guan – Key Laboratory of Livestock Infectious Diseases, Ministry of Education, Key Laboratory of Ruminant Infectious Disease Prevention and Control (East), Ministry of Agriculture and Rural Affairs, College of Animal Science and Veterinary Medicine, Shenyang Agricultural University, Shenyang, Liaoning 110866, China

Zhen-Chi Zhou – Key Laboratory of Livestock Infectious Diseases, Ministry of Education, Key Laboratory of Ruminant Infectious Disease Prevention and Control (East), Ministry of Agriculture and Rural Affairs, College of Animal Science and Veterinary Medicine, Shenyang Agricultural University, Shenyang, Liaoning 110866, China

Jie Wu – Key Laboratory of Livestock Infectious Diseases, Ministry of Education, Key Laboratory of Ruminant Infectious Disease Prevention and Control (East), Ministry of Agriculture and Rural Affairs, College of Animal Science and Veterinary Medicine, Shenyang Agricultural University, Shenyang, Liaoning 110866, China

Ming-Yue Zhao – College of Food Science, National R&D Professional Center For Berry Processing, National Engineering and Technology of Research Center For Small berry, Key Laboratory of Healthy Food Nutrition and Innovative Manufacturing, Liaoning Province, Shenyang Agricultural University, Shenyang, Liaoning 110866, China

Yue Li – College of Food Science, National R&D Professional Center For Berry Processing, National Engineering and Technology of Research Center For Small berry, Key Laboratory of Healthy Food Nutrition and Innovative Manufacturing, Liaoning Province, Shenyang Agricultural University, Shenyang, Liaoning 110866, China

Han-Xiao Liu – College of Food Science, National R&D Professional Center For Berry Processing, National Engineering and Technology of Research Center For Small berry, Key Laboratory of Healthy Food Nutrition and Innovative Manufacturing, Liaoning Province, Shenyang Agricultural University, Shenyang, Liaoning 110866, China

Complete contact information is available at:
<https://pubs.acs.org/10.1021/acs.jafc.3c00776>

Author Contributions

[†]J.-L.T. and M.Z. contributed equally to this work as co-first authors.

Funding

This work was supported by the National Natural Science Foundation of China (32202074), the Science Research Fund Project of Liaoning Provincial Department of Education (grant no. LJKZ0667), and the Scientific Research Foundation of Shenyang Agricultural University (grant nos. 880415026 and 880418027).

Notes

The authors declare no competing financial interest.

REFERENCES

- (1) Li, Z.; Tian, J.; Cheng, Z.; Teng, W.; Zhang, W.; Bao, Y.; Wang, Y.; Song, B.; Chen, Y.; Li, B. Hypoglycemic bioactivity of anthocyanins: a review on proposed targets and potential signaling pathways. *Crit. Rev. Food Sci. Nutr.* **2022**, 1–18.
- (2) Aschner, P.; Karuranga, S.; James, S.; Simmons, D.; Basit, A.; Shaw, J. E.; Wild, S. H.; Ogurtsova, K.; Saedi, P.; International Diabetes Federation's Diabetes Epidemiological Guide Writing Group. The international diabetes federation's guide for diabetes epidemiological studies. *Diabetes Res. Clin. Pract.* **2021**, 172, No. 108630.
- (3) Tian, J. L.; Si, X.; Shu, C.; Wang, Y. H.; Tan, H.; Zang, Z. H.; Zhang, W. J.; Xie, X.; Chen, Y.; Li, B. Synergistic effects of combined anthocyanin and metformin treatment for hyperglycemia *in vitro* and *in vivo*. *J. Agric. Food Chem.* **2022**, 70, 1182–1195.
- (4) Lutz, T. A. Mammalian models of diabetes mellitus, with a focus on type 2 diabetes mellitus. *Nat. Rev. Endocrinol.* **2023**, 350.

- (5) Hu, P.; Li, D. H.; Jia, C. C.; Liu, Q.; Wang, X. F.; Li, Z. L.; Hua, H. M. Bioactive constituents from *Vitex negundo* var. *heterophylla* and their antioxidant and α -glucosidase inhibitory activities. *J. Funct. Foods* **2017**, 35, 236–244.

- (6) Naveen, Y. P.; Asna, U.; Kullaiah, B. A review on medicinal plants evaluated for anti-diabetic potential in clinical trials: Present status and future perspective. *J. Herb. Med.* **2021**, 28, No. 100436.

- (7) Miao, L.; Liu, C.; Cheong, M. S.; Zhong, R.; Tan, Y.; Rengasamy, K. R. R.; Leung, S. W. S.; Cheang, W. S.; Xiao, J. Exploration of natural flavones' bioactivity and bioavailability in chronic inflammation induced-type-2 diabetes mellitus. *Crit. Rev. Food Sci.* **2022**, 1–28.

- (8) Hu, T. G.; Wen, P.; Shen, W. Z.; Liu, F.; Li, Q.; Li, E. N.; Liao, S. T.; Wu, H.; Zou, Y. X. Effect of 1-deoxyojirimycin isolated from mulberry leaves on glucose metabolism and gut microbiota in a streptozotocin-induced diabetic mouse model. *J. Nat. Prod.* **2019**, 82, 2189–2200.

- (9) Dat, N. T.; Binh, P. T. X.; Quynh, L. T. P.; Minh, C. V.; Huong, H. T.; Lee, J. J. Cytotoxic prenylated flavonoids from *Morus alba*. *Fitoterapia* **2010**, 81, 1224–1227.

- (10) He, X.; Fang, J.; Ruan, Y.; Wang, X.; Sun, Y.; Wu, N.; Zhao, Z.; Chang, Y.; Ning, N.; Guo, H.; Huang, L. Structures, bioactivities and future prospective of polysaccharides from *Morus alba* (white mulberry): a review. *Food Chem.* **2018**, 245, 899–910.

- (11) Ma, G.; Chai, X.; Hou, G.; Zhao, F.; Meng, Q. Phytochemistry, bioactivities and future prospects of mulberry leaves: a review. *Food Chem.* **2022**, 372, No. 131335.

- (12) China Pharmacopoeia Commission. *Chinese pharmacopoeia*; China medical science press: Beijing 2020.

- (13) Sánchez-Salcedo, E. M.; Mena, P.; García-Viguera, C.; Hernández, F.; Martínez, J. J. (Poly)phenolic compounds and antioxidant activity of white (*Morus alba*) and black (*Morus nigra*) mulberry leaves: their potential for new products rich in phytochemicals. *J. Funct. Foods* **2015**, 18, 1039–1046.

- (14) Niu, S. L.; Tong, Z. F.; Zhang, Y.; Liu, T. L.; Tian, C. L.; Zhang, D. X.; Liu, M. C.; Li, B.; Tian, J. L. Novel protein tyrosine phosphatase 1B inhibitor-geranylated flavonoid from mulberry leaves ameliorates insulin resistance. *J. Agric. Food Chem.* **2020**, 68, 8223–8231.

- (15) Tian, J. L.; Si, X.; Wang, Y. H.; Gong, E. S.; Xie, X.; Zhang, Y.; Li, B.; Shu, C. Bioactive flavonoids from *Rubus corchorifolius* inhibit α -glucosidase and α -amylase to improve postprandial hyperglycemia. *Food Chem.* **2021**, 341, No. 128149.

- (16) Asai, T.; Hara, N.; Kobayashi, S.; Kohshima, S.; Fujimoto, Y. Geranylated flavanones from the secretion on the surface of the immature fruits of *Paulownia tomentosa*. *Phytochemistry* **2008**, 69, 1234–1241.

- (17) Fukai, T.; Pei, Y.-H.; Nomura, T.; Xu, C.-Q.; Wu, L.-J.; Chen, Y.-J. Components of the root bark of *Morus cathayana*. 1. Structures of five new isoprenylated flavonoids, sanggenols A - E and a diprenyl-2-arylbenzofuran, mulberrofuran V. *Heterocycles* **1996**, 43, 425–436.

- (18) Slade, D.; Ferreira, D.; Marais, J. P. J. Circular dichroism, a powerful tool for the assessment of absolute configuration of flavonoids. *Phytochemistry* **2005**, 66, 2177–2215.

- (19) Jung, J. W.; Park, J. H.; Lee, Y. G.; Seo, K. H.; Oh, E. J.; Lee, D. Y.; Lim, D. W.; Han, D.; Baek, N. I. Three new isoprenylated flavonoids from the root bark of *Morus alba*. *Molecules* **2016**, 21, 1112.

- (20) Kim, J. Y.; Lee, W. S.; Kim, Y. S.; Curtis-Long, M. J.; Lee, B. W.; Ryu, Y. B.; Park, K. H. Isolation of cholinesterase-inhibiting flavonoids from *Morus lhou*. *J. Agric. Food Chem.* **2011**, 59, 4589–4596.

- (21) Qu, K. J.; Wang, B.; Jiang, C. S.; Xie, B. G.; Liu, A. H.; Li, S. W.; Guo, Y. W.; Li, J.; Mao, S. C. Rearranged Diels–Alder Adducts and Prenylated Flavonoids as Potential PTP1B Inhibitors from *Morus nigra*. *J. Nat. Prod.* **2021**, 84, 2303–2311.

- (22) Hao, M.; Huang, P.; Ruan, J.; Sun, F.; Han, L.; Liu, M.; Zhang, Y.; Wang, T. Bioactive flavonoids and stilbenes from the leaf of *Morus alba* var. *multicaulis*. *Fitoterapia* **2021**, 154, No. 105018.

- (23) Lee, D.; Bhat, K. P. L.; Fong, H. H. S.; Farnsworth, N. R.; Pezzuto, J. M.; Kinghorn, A. D. Aromatase inhibitors from *Broussonetia papyrifera*. *J. Nat. Prod.* **2001**, 64, 1286–1293.

- (24) Zheng, Z. P.; Cheng, K. W.; Zhu, Q.; Wang, X. C.; Lin, Z. X.; Wang, M. Tyrosinase inhibitory constituents from the roots of *Morus nigra*: A structure–activity relationship study. *J. Agric. Food Chem.* **2010**, *58*, 5368–5373.
- (25) Hano, Y.; Nomura, T. Constituents of the chinese crude drug “sang-bai-pi” (*Morus* root barks) iv. structures of four new flavonoids, sanggenon H, I, J and K. *Heterocycles* **1983**, *20*, 1071–1076.
- (26) Tian, J. L.; Liao, X. J.; Wang, Y. H.; Si, X.; Shu, C.; Gong, E. S.; Xie, X.; Ran, X. L.; Li, B. Identification of cyanidin-3-arabinoside extracted from blueberry as a selective protein tyrosine phosphatase 1B inhibitor. *J. Agric. Food Chem.* **2019**, *67*, 13624.
- (27) Xu, Y.; Rashwan, A. K.; Ge, Z.; Li, Y.; Ge, H.; Li, J.; Xie, J.; Liu, S.; Fang, J.; Cheng, K.; Chen, W. Identification of a novel α -glucosidase inhibitor from *Melastoma dodecandrum* Lour. fruits and its effect on regulating postprandial blood glucose. *Food Chem.* **2023**, *399*, No. 133999.
- (28) Ross, P. D.; Subramanian, S. Thermodynamics of protein association reactions: Forces contributing to stability. *Biochemistry* **1981**, *20*, 3096–3102.
- (29) Ji, Y.; Liu, D.; Jin, Y.; Zhao, J.; Zhao, J.; Li, H.; Li, L.; Zhang, H.; Wang, H. *In vitro* and *in vivo* inhibitory effect of anthocyanin-rich bilberry extract on α -glucosidase and α -amylase. *LWT–Food Sci. Technol.* **2021**, *145*, No. 111484.
- (30) Xue, B.; Tian, J.; Wang, Y.; Jin, B.; Deng, H.; Gao, N.; Xie, X.; Tang, S.; Li, B. Mechanism underlying the interaction of malvidin-3-O-galactoside with protein tyrosine phosphatase-1B and α -glucosidase. *J. Mol. Struct.* **2022**, *1253*, No. 132249.
- (31) Liu, B.-R.; Zheng, H.-R.; Jiang, X.-J.; Zhang, P.-Z.; Wei, G.-Z. Serratene triterpenoids from *Lycopodium cernuum* L. as α -glucosidase inhibitors: Identification, structure–activity relationship and molecular docking studies. *Phytochemistry* **2022**, *195*, No. 113056.
- (32) Hou, C.; Shi, C.; Ren, J. Xanthine oxidase targeted model setup and its application for antihyperuricemic compounds prediction by *in silico* methods. *eFood.* **2021**, *2*, 296–306.
- (33) Wang, L.; Zhang, Y.; Johnpaul, I. A.; Hong, K.; Song, Y.; Xiao, Y.; Lv, C.; Ma, C. Exploring two types of prenylated bitter compounds from hop plant (*Humulus lupulus* L.) against α -glucosidase *in vitro* and *in silico*. *Food Chem.* **2022**, *370*, No. 130979.
- (34) Chouhan, H.; Purohit, A.; Ram, H.; Chowdhury, S.; Kashyap, P.; Panwar, A.; Kumar, A. The interaction capabilities of phytoconstituents of ethanolic seed extract of cumin (*Cuminum cyminum* L.) with HMG-CoA reductase to subside the hypercholesterolemia: A mechanistic approach. *Food Front.* **2021**, *3*, 300–315.
- (35) De Oliveira, T. V.; Polêto, M. D.; Barbosa, S. V.; dos Reis Coimbra, J. S.; De Oliveira, E. B. Impacts of Ca^{2+} cation and temperature on bovine α -lactalbumin secondary structures and foamability—insights from computational molecular dynamics. *Food Chem.* **2022**, *367*, No. 130733.
- (36) Li, Y.; Yuan, Z.; Gao, Y.; Bao, Z.; Sun, N.; Lin, S. Mechanism of trypsin activation by pulsed electric field treatment revealed based on chemical experiments and molecular dynamics simulations. *Food Chem.* **2022**, *394*, No. 133477.
- (37) Da Silva, C. G.; Duque, M. D.; Nordi, C. S. F.; Viana-Niero, C. New insights into toxicity of microcystins produced by cyanobacteria using *in silico* ADMET prediction. *Toxicol.* **2021**, *204*, 64–71.
- (38) Zhong, R.; Farag, M. A.; Chen, M.; He, C.; Xiao, J. Recent advances in the biosynthesis, structure–activity relationships, formulations, pharmacology, and clinical trials of fisetin. *eFood.* **2022**, *3*, No. e3.
- (39) Yang, L.; Gao, Y.; Gong, J.; Wang, H.; Farag, M. A.; Simal-Gandara, J.; Zhao, Y.; Nie, S.; Xiao, J. Myricetin ameliorated prediabetes via immunomodulation and gut microbiota interaction. *Food Front.* **2022**, *3*, 749–772.
- (40) Tabopda, T. K.; Ngoupayo, J.; Awoussong, P. K.; Mitaine-Offer, A.-C.; Ali, M. S.; Ngadjui, B. T.; Lacaille-Dubois, M. Triprenylated flavonoids from *Dorstenia ptilurus* and their α -glucosidase inhibition properties. *J. Nat. Prod.* **2008**, *71*, 2068–2072.
- (41) Yu, Y.; Xu, S.; He, R.; Liang, G. Application of Molecular Simulation Methods in Food Science: Status and Prospects. *J. Agric. Food Chem.* **2023**, *71*, 2684–2703.
- (42) Li, B.; Fu, R.; Tan, H.; Zhang, Y.; Teng, W.; Li, Z.; Tian, J. Characteristics of the interaction mechanisms of procyanidin B1 and procyanidin B2 with protein tyrosine phosphatase-1B: analysis by kinetics, spectroscopy methods and molecular docking. *Spectrochim. Acta, Part A* **2021**, *259*, No. 119910.
- (43) Lang, Y.; Gao, H.; Tian, J.; Shu, C.; Sun, R.; Li, B.; Meng, X. Protective effects of α -casein or β -casein on the stability and antioxidant capacity of blueberry anthocyanins and their interaction mechanism. *LWT–Food Sci. Technol.* **2019**, *115*, No. 108434.
- (44) Khalifa, M. M.; Sakr, H. M.; Ibrahim, A.; Mansour, A. M.; Ayyad, R. R. Design and synthesis of new benzylidene-quinazolinone hybrids as potential anti-diabetic agents: *In vitro* α -glucosidase inhibition, and docking studies. *J. Mol. Struct.* **2022**, *1250*, No. 131768.
- (45) Abdulhakim, J. A. Effect of guggulsterone, a sterol identified in *Commiphora gileadensis* (Becham), on the dengue virus enzymes: Pharmacokinetics, molecular docking and molecular dynamics simulations studies. *J. King Saud Univ., Sci.* **2022**, *34*, No. 102140.